ANNUAL REVIEWS

Annual Review of Physical Chemistry

Path Integrals for Nonadiabatic Dynamics: Multistate Ring Polymer Molecular Dynamics

Nandini Ananth

Department of Chemistry and Chemical Biology, Cornell University, Ithaca, New York, USA; email: ananth@cornell.edu

Keywords

nonadiabatic dynamics, path integrals, semiclassical theory, mapping variables, real-time correlation functions, excited-state dynamics

Abstract

This review focuses on a recent class of path-integral-based methods for the simulation of nonadiabatic dynamics in the condensed phase using only classical molecular dynamics trajectories in an extended phase space. Specifically, a semiclassical mapping protocol is used to derive an exact, continuous, Cartesian variable path-integral representation for the canonical partition function of a system in which multiple electronic states are coupled to nuclear degrees of freedom. Building on this exact statistical foundation, multistate ring polymer molecular dynamics methods are developed for the approximate calculation of real-time thermal correlation functions. The remarkable promise of these multistate ring polymer methods, their successful applications, and their limitations are discussed in detail.

1. INTRODUCTION

Coupled electron–nuclear motion, nonadiabatic effects, are ubiquitous in chemistry and play a key role in the transport of spin, charge, energy, and excitation through complex molecular systems (1, 2). Adiabatic or Born-Oppenheimer dynamics describe the time evolution of the nuclear wave function under forces from a single electronic potential energy surface (3). Nonadiabatic processes, in which the Born-Oppenheimer approximation is no longer valid, correspond to nuclear dynamics on multiple, coupled electronic potential energy surfaces that are not well-separated energetically. It is this need to include more than one electronic state that offers a challenge to theory: Accurate and rapid electronic structure methods are required to characterize multiple electronic states (typically the ground state and a handful of low-lying excited states) accompanied by quantum dynamic methods that can capture the coupling between nuclear motion and electronic state transitions.

Great strides have been made in the development of exact quantum dynamic methods (4–8); however, large-scale and predictive simulations of nonadiabatic processes remain a significant challenge. Nonadiabatic methods based on Gaussian wave packet dynamics (9, 10) and semiclassical theory have had some success in small system simulations (11–14), with the linearized semiclassical initial value representation (LSC-IVR) (15–21) and the recently introduced quasiclassical windowing methods (22–24) showing the most promise for higher-dimensional system studies. Similarly, rigorous mixed quantum classical approximations for nonadiabatic dynamics derived from first principles enable studies on systems with a handful of degrees of freedom (25–28), but it is the more ad hoc surface hopping approach that is, arguably, the most widely used for large-scale simulations (29–34). Unfortunately, standard surface hopping simulations of high-dimensional condensed-phase systems face challenges due to the lack of nuclear quantization, the differential treatment of electronic and nuclear dynamics, and the use of dynamics that do not preserve detailed balance (31).

Centroid molecular dynamics (CMD) (35–38) and ring polymer molecular dynamics (RPMD) (39–41) have emerged as a particularly successful class of methods for condensed-phase simulations of Born-Oppenheimer dynamics. Both of these approaches are based on exact, imaginary-time path integrals (42, 43) and have been shown to successfully describe nuclear quantum effects in condensed-phase quantum systems using only classical molecular dynamics trajectories. In particular, RPMD has been used in large-scale atomistic simulations of charge transfer (44–49). The broad success of RPMD has motivated the development of several approximate, imaginary-time, path-integral-based methods for quantum dynamic simulations of nonadiabatic reactions. This includes the mapping-variable (MV)-RPMD method that, like RPMD, employs an ensemble of classical trajectories to preserve the quantum Boltzmann distribution (50–54) and the closely related nonadiabatic RPMD (NRPMD) (55–58) and coherent-state (CS)-RPMD (59).

This review showcases the development of multistate RPMD methods, highlighting their promise for efficient, accurate, and predictive simulations of nonadiabatic processes. Current theoretical limitations and implementation challenges are also discussed, along with some directions for future development. Readers of this review might find it helpful to refresh their understanding of nonadiabatic dynamics and conical intersections (60) as well as RPMD (41).

2. THEORY

2.1. Nonadiabatic Dynamics

The molecular Hamiltonian for a system of electrons and nuclei can be written as

$$\hat{H}(\mathbf{r}, \mathbf{R}) = \hat{T}_R + \hat{H}_{el}(\mathbf{r}, \mathbf{R}), \qquad 1.$$

where $\hat{T}_R$ is the nuclear kinetic energy operator and $\hat{H}_{el}(\mathbf{r}, \mathbf{R})$ is the electronic Hamiltonian. The eigenfunctions of the total molecular Hamiltonian can then be written as an expansion,

$$\Psi(\mathbf{r}, \mathbf{R}, t) = \sum_j \chi_j(\mathbf{R}, t)\phi_j(\mathbf{r}, \mathbf{R}), \qquad 2.$$

where the coefficients of expansion are the time-dependent nuclear wave functions, $\chi_j(\mathbf{R}, t)$, and $\phi_j(\mathbf{r}, \mathbf{R})$ is the complete orthonormal set of eigenfunctions obtained by solving the time-independent electronic Schrödinger equation,

$$\hat{H}_{el}\phi_j(\mathbf{r}, \mathbf{R}) = E_j(\mathbf{R})\phi_j(\mathbf{r}, \mathbf{R}). \qquad 3.$$

The total molecular wave function evolves in time according to the time-dependent Schrödinger equation,

$$i\hbar \frac{\partial \Psi(\mathbf{r}, \mathbf{R}, t)}{\partial t} = \hat{H}\Psi(\mathbf{r}, \mathbf{R}, t), \qquad 4.$$

which can be further simplified to obtain equations of motion for the nuclear wave function,

$$i\hbar \frac{\partial \chi_j(\mathbf{R}, t)}{\partial t} = \left[\hat{T}_R + E_j(\mathbf{R})\right]\chi_j(\mathbf{R}, t) + \sum_k C_{jk}\chi_k(\mathbf{R}, t). \qquad 5.$$

Equation 5 describes coupled nonadiabatic motion of the nuclear wave function $\chi_j(\mathbf{R}, t)$: The first term in brackets defines motion on a single electronic potential energy surface $E_j(\mathbf{R})$ and the second term describes coupled motion through the nonadiabatic coupling operator,

$$C_{jk} = \langle\phi_j|\hat{T}_R|\phi_k\rangle - \sum_i \frac{\hbar^2}{M_i} \langle\phi_j|\nabla_i|\phi_k\rangle \nabla_i, \qquad 6.$$

where the nuclear kinetic operator is $\hat{T}_R = -\sum_i \frac{\hbar^2}{2M_i}\nabla_i^2$, and the summation index i runs over the number of nuclear degrees of freedom. Born-Oppenheimer dynamics (sometimes referred to as adiabatic dynamics) assumes that the nonadiabatic coupling is negligible, i.e., $C_{jk} \approx 0$, resulting in a significantly simpler equation that describes nuclear motion on a single electronic surface (3). This section describes nonadiabatic dynamics in the adiabatic representation; in the next section, I introduce the diabatic Hamiltonian. See the sidebar titled Adiabatic and Diabatic Representations for more information.

2.2. Mapping Variables for Electronic States

Developing classical trajectory-based methods for nonadiabatic dynamics requires transforming from discrete electronic states to continuous Cartesian electronic variables. This idea has been explored extensively in the semiclassical literature, and several formally exact mappings have been proposed (11, 12, 61, 62). This review confines itself to the Meyer-Miller-Stock-Thoss (MMST) mapping that has been shown to work well for a wide range of applications (13, 18, 19, 63, 64).

   The MMST mapping was first introduced as a mapping from discrete electronic state variables to classical analog action-angle variables (11, 65) and was subsequently established to be an exact transformation (12). Specifically, electronic states are mapped to bosonic creation and annihilation operators with commutation relations $[a_n^\dagger, a_m] = \delta_{nm}$:

$$|\psi_n\rangle \langle\psi_m| \rightarrow \hat{a}_n^\dagger \hat{a}_m = \frac{1}{\sqrt{2\hbar}} ([\hat{\mathbf{x}}]_n - i[\hat{\mathbf{p}}]_n) \frac{1}{\sqrt{2\hbar}} ([\hat{\mathbf{x}}]_m + i[\hat{\mathbf{p}}]_m). \qquad 7.$$

In Equation 7, $[.]_n$ indicates the nth element of the K-dimensional electronic position and momentum operators $\hat{\mathbf{x}}$ and $\hat{\mathbf{p}}$, and the equality is obtained using the definitions of the ladder operators.

ADIABATIC AND DIABATIC REPRESENTATIONS

In general, the complete set of eigenfunctions of the electronic Hamiltonian, $\{\phi_j(\mathbf{r}, \mathbf{R})\}$, is referred to as the adiabatic representation, and, as discussed in Section 2.1, nuclear motion is coupled to the adiabatic electronic states through the nonadiabatic coupling vector. This vector is challenging to compute for high-dimensional systems, and its magnitude is inversely proportional to the energetic separation between electronic states, making it singular at conical intersections.

The diabatic representation $\hat{H}$ is constructed to minimize the nonadiabatic coupling vector. However, the resulting states are not eigenstates of the electronic Hamiltonian leading to off-diagonal terms in the potential energy matrix. Diabatic states are frequently localized, providing an intuitive physical picture of reactive events: For instance, the donor state and the acceptor state in an electron-transfer reaction are, typically, diabats.

Diabatic states are nonunique, and several diabatization protocols have been developed to construct quasi-diabatic states either by transforming from an adiabatic basis or through direct localization protocols (66–74). The multistate RPMD methods discussed here are all derived assuming a diabatic representation.

The K electronic states of the system are thus mapped to a set of K singly excited oscillator (SEO) states,

$$|\psi_n\rangle \rightarrow |0_1 0_2 \ldots 1_n \ldots 0_K\rangle \equiv |n\rangle, \qquad 8.$$

that are defined as the product of $K - 1$ independent ground-state harmonic oscillators and one oscillator in the first excited state. In Equation 8, the notation $|n\rangle$ is introduced for the SEO states, indicating that the nth oscillator is singly excited. As a simple example, the electronic states of a two-level system can be mapped to two SEO states, $|1\rangle$ and $|2\rangle$, such that

$$\psi_1 \rightarrow |1\rangle \equiv |1_1 0_2\rangle \ \text{and} \ \psi_2 \rightarrow |2\rangle \equiv |0_1 1_2\rangle. \qquad 9.$$

Note that the mapping defined here is exact for both adiabatic and diabatic states (11, 18).

Consider a diabatic Hamiltonian for a system with K electronic states and F nuclear degrees of freedom,

$$\hat{H} = \frac{1}{2}\hat{\mathbf{P}}^T \mathbf{M}^{-1}\hat{\mathbf{P}} + V_0(\hat{\mathbf{R}}) + \sum_{n,m=1}^{K} |\psi_n\rangle \, [\mathbf{V}_e]_{nm}(\hat{\mathbf{R}}) \, \langle\psi_m|, \qquad 10.$$

where $\mathbf{R}$ and $\mathbf{P}$ are the F-dimensional vectors of nuclear positions and momenta, $\mathbf{M}$ is the diagonal mass matrix, $V_0(\mathbf{R})$ is the state-independent potential energy, $[\mathbf{V}_e]_{nm}(\mathbf{R})$ are elements of the $K \times K$ diabatic potential energy matrix, and $|\psi_n\rangle$ are the diabatic electronic states. Using the mapping in Equation 7, the K-state Hamiltonian in Equation 10 can be written in the SEO basis as

$$\hat{H} = \frac{1}{2}\hat{\mathbf{P}}^T \mathbf{M}^{-1}\hat{\mathbf{P}} + V_0(\hat{\mathbf{R}}) + \sum_{n,m=1}^{K} |n\rangle \, [\mathbf{V}_e]_{nm}(\hat{\mathbf{R}}) \, \langle m|, \qquad 11.$$

or equivalently in Cartesian operator form as

$$\hat{H}_{\mathrm{mmst}} = \frac{1}{2}\hat{\mathbf{P}}^T \mathbf{M}^{-1}\hat{\mathbf{P}} + V_0(\hat{\mathbf{R}}) + \frac{1}{2}\sum_{n,m=1}^{K} [\mathbf{V}_e]_{nm}(\hat{\mathbf{R}}) \left([\hat{\mathbf{x}}]_n [\hat{\mathbf{x}}]_m + [\hat{\mathbf{p}}]_n [\hat{\mathbf{p}}]_m - \delta_{nm}\hbar\right). \qquad 12.$$

Approximate semiclassical methods for nonadiabatic dynamics such as LSC-IVR (15–17, 19) typically use classical trajectories generated by the classical version of the Hamiltonian in

Equation 12,

$$\dot{\mathbf{R}} = \frac{\partial H_{\mathrm{mmst}}}{\partial \mathbf{P}} \quad \dot{\mathbf{P}} = -\frac{\partial H_{\mathrm{mmst}}}{\partial \mathbf{R}},$$

$$[\dot{\mathbf{x}}]_n = \frac{\partial H_{\mathrm{mmst}}}{\partial [\mathbf{p}]_n} \quad [\dot{\mathbf{p}}]_n = -\frac{\partial H_{\mathrm{mmst}}}{\partial [\mathbf{x}]_n}. \qquad 13.$$

2.3. Imaginary-Time Path Integrals for a Multistate System

The path-integral representation yields an exact classically isomorphic representation of the quantum canonical partition function (42). Here, I introduce the modifications necessary to construct an exact path-integral representation for the canonical partition function of a multistate system using the mapping variables (MVs).

Consider the quantum mechanical partition function for a canonical ensemble,

$$Z = \mathrm{Tr}\left[e^{-\beta \hat{H}}\right] = \sum_{n=1}^{K} \int d\mathbf{R} \langle \mathbf{R}, \psi_n | e^{-\beta \hat{H}} | \mathbf{R}, \psi_n \rangle, \qquad 14.$$

where $\hat{H}$ is the diabatic Hamiltonian in Equation 10, $\beta = 1/k_B T$, $|\mathbf{R}\rangle$ represent nuclear position states, and $|\psi_n\rangle$ are the diabatic electronic states. Inserting N copies of the identity operator,

$$\hat{\mathbb{1}} = \sum_{n=1}^{K} \int d\mathbf{R} |\mathbf{R}, \psi_n\rangle \langle \mathbf{R}, \psi_n |, \qquad 15.$$

we obtain a product of high-temperature matrix elements in the electronic and nuclear degrees of freedom,

$$Z = \lim_{N \to \infty} \int d\mathbf{R}_1 \int d\mathbf{R}_2 \ldots \int d\mathbf{R}_N \prod_{\alpha=1}^{K} \langle \mathbf{R}_\alpha | e^{-\beta_N \hat{H}_0} | \mathbf{R}_{\alpha+1} \rangle \times I_{\mathrm{el}}, \qquad 16.$$

where $\beta_N = \beta/N$, the state-independent Hamiltonian, $\hat{H}_0 = \frac{1}{2}\hat{\mathbf{P}}^T \mathbf{M}^{-1}\hat{\mathbf{P}} + V_0(\hat{\mathbf{R}})$, and the electronic trace is defined as

$$I_{\mathrm{el}} = \sum_{n_1} \sum_{n_2} \cdots \sum_{n_N} \prod_{\alpha=1}^{N} \langle \psi_{n_\alpha} | e^{-\beta_N \mathbf{V}_e(\mathbf{R}_\alpha)} | \psi_{n_{\alpha+1}} \rangle. \qquad 17.$$

Note that in Equations 16 and 17, the multistate ring polymer is cyclic, with $\mathbf{R}_{N+1} = \mathbf{R}_1$ and $\psi_{n_{N+1}} = \psi_{n_1}$. The high-temperature nuclear matrix elements can be evaluated within the Suzuki-Trotter approximation (75, 76) to obtain a nuclear phase-space integral expression for the quantum canonical partition function,

$$Z \propto \lim_{N \to \infty} \int d\{\mathbf{R}, \mathbf{P}\} e^{-\beta_N H_{\mathrm{rp}}(\{\mathbf{R}, \mathbf{P}\})} \times I_{\mathrm{el}}, \qquad 18.$$

where the notation $\int d\{\mathbf{R}, \mathbf{P}\} \equiv \int d\mathbf{R}_1 \int d\mathbf{P}_1 \ldots \int d\mathbf{R}_N \int d\mathbf{P}_N$ is introduced, and the proportionality sign indicates that some constants have been omitted. The classical nuclear ring polymer Hamiltonian in Equation 18 is

$$H_{\mathrm{rp}}(\{\mathbf{R}, \mathbf{P}\}) = \sum_{\alpha=1}^{N} \frac{1}{2} \mathbf{P}_\alpha^T \mathbf{M}^{-1} \mathbf{P}_\alpha + V_{\mathrm{rp}}(\{\mathbf{R}\}), \qquad 19.$$

with the ring polymer potential defined as

$$V_{\mathrm{rp}} = \sum_{\alpha=1}^{N} \frac{1}{2} \omega_N^2 (\mathbf{R}_\alpha - \mathbf{R}_{\alpha+1})^T \mathbf{M} (\mathbf{R}_\alpha - \mathbf{R}_{\alpha+1}) + V_0(\mathbf{R}_\alpha), \qquad 20.$$

and $\omega_N = N/(\beta\hbar)$. The different multistate path-integral-based methods discussed in this review differ in their treatment of the electronic integral in Equation 17.

2.3.1. Mean-field formulation.
The high-temperature electronic matrix elements in Equation 17,

$$\langle \psi_n | e^{-\beta_N \mathbf{V}_e(\mathbf{R}_\alpha)} | \psi_m \rangle = [\mathbf{\Gamma}]_{nm}(\mathbf{R}_\alpha), \qquad 21.$$

can be either calculated by diagonalizing the diabatic potential energy matrix when K is small or analytically evaluated in the $N \to \infty$ limit (77),

$$[\mathbf{\Gamma}]_{nm}(\mathbf{R}) = \begin{cases} e^{-\beta_N V_{nn}(\mathbf{R})} & \text{if } n = m \\ (-\beta_N V_{nm}) e^{-\beta_N V_{nn}(\mathbf{R})} & \text{if } n \neq m \end{cases}. \qquad 22.$$

Substituting Equation 22 into Equations 17 and 18, we obtain an exact, mean-field (MF) path-integral representation of the canonical partition function,

$$Z \propto \lim_{N \to \infty} \int d\{\mathbf{R}, \mathbf{P}\} \, e^{-\beta_N H_{\mathrm{mf}}(\{R\})} \mathrm{sgn}(\Theta_{\mathrm{mf}}), \qquad 23.$$

where the MF ring polymer Hamiltonian is defined as

$$H_{\mathrm{mf}}(\{\mathbf{R}\}, \{\mathbf{P}\}) = \sum_{\alpha=1}^{N} \frac{1}{2} \mathbf{P}_\alpha^T \mathbf{M}^{-1} \mathbf{P}_\alpha + V_{\mathrm{rp}}(\{\mathbf{R}\}) - \frac{1}{\beta_N} \ln(|\Theta_{\mathrm{mf}}(\{\mathbf{R}\})|), \qquad 24.$$

and the effective state-averaged potential is obtained from

$$\Theta_{\mathrm{mf}} = \mathrm{Tr}\left[\prod_{\alpha=1}^{N} \mathbf{\Gamma}(\mathbf{R}_\alpha)\right], \qquad 25.$$

where the $K \times K$ matrix elements of $\mathbf{\Gamma}$ are as defined in Equation 22. Note that it is necessary to include the sign function in Equation 24, as Θ_{mf} is not necessarily positive for systems with $K > 2$.

In the MF framework, nuclei are time-evolved by integrating the classical equations of motion under the MF Hamiltonian in Equation 24,

$$\dot{\mathbf{R}}_\alpha = \frac{\partial H_{\mathrm{mf}}}{\partial \mathbf{P}_\alpha} \quad \text{and} \quad \dot{\mathbf{P}}_\alpha = -\frac{\partial H_{\mathrm{mf}}}{\partial \mathbf{R}_\alpha}. \qquad 26.$$

These trajectories, generated in a standard path-integral molecular dynamics (PIMD) simulation (78), are then used to calculate exact thermal equilibrium average properties for a multistate system.

2.3.2. Electronic mapping variable path integral.
Deriving a classically isomorphic path-integral expression for the electronic integral in Equation 17 using explicit MVs requires a new discretization protocol. Specifically, the discrete diabatic state identity operator in Equation 15 must be replaced with an identity defined in electronic position states (79)

$$\hat{1} = \int d\mathbf{x} \, |\mathbf{x}\rangle \langle \mathbf{x}| \, \hat{\mathcal{P}}, \qquad 27.$$

where the projection operator, $\hat{\mathcal{P}}$, constrains the electronic MVs to the SEO basis,

$$\hat{\mathcal{P}} = \sum_{n=1}^{K} |n\rangle \langle n|. \qquad 28.$$

Inserting N copies of this identity leads to an electronic integral of the form

$$I_{el} = \int d\mathbf{x}_1 \int d\mathbf{x}_2 \dots \int d\mathbf{x}_N \prod_{\alpha=1}^{N} \langle \mathbf{x}_\alpha | \hat{\mathcal{P}} e^{-\beta_N \mathbf{V}_e(\mathbf{R}_\alpha)} \hat{\mathcal{P}} | \mathbf{x}_{\alpha+1} \rangle. \qquad 29.$$

Using the definition of the SEO states and evaluating the matrix elements within the high-temperature Trotter approximation (80) yield an expression for the multistate partition function (79):

$$Z \propto \lim_{N \to \infty} \int d\{\mathbf{R}, \mathbf{P}\} \int d\{\mathbf{x}\}\, e^{-\beta_N H_{rp}} e^{-\sum_{\alpha=1}^{N} \mathbf{x}_\alpha^T \cdot \mathbf{x}_\alpha}\, \Theta_0\left(\{\mathbf{x}\}, \{\mathbf{R}\}\right). \qquad 30.$$

In Equation 30, H_{rp} is previously defined in Equation 19, and the electron-nuclear coupling term is

$$\Theta_0\left(\mathbf{x}, \mathbf{R}\right) = \mathrm{Tr}\left[\prod_{\alpha=1}^{N} \left(\mathbf{x}_\alpha \otimes \mathbf{x}_\alpha^T\right) \boldsymbol{\Gamma}(\mathbf{R}_\alpha)\right]. \qquad 31.$$

In Equation 31, the symbol $\otimes$ is used to represent an outer product of the K-dimensional electronic position vectors. Exact thermal equilibrium properties can be computed for K-level systems using standard path-integral Monte Carlo (PIMC) importance sampling (81).

Deriving a classically isomorphic representation for the canonical partition function requires an integral over a phase-space distribution for both the electronic and nuclear degrees of freedom. The next section discusses some of the different ways in which such an electronic phase-space distribution can be generated.

2.4. Approximate Real-Time Correlation Functions

Classical configurations drawn from an exact N-bead imaginary time path integral distribution can be time evolved under an effective classical Hamiltonian to approximately calculate the real-time correlation functions of a quantum system.

2.4.1. Ring polymer molecular dynamics.
For an adiabatic (single-surface) process, the path-integral representation of the canonical partition function in Equation 18 simplifies to

$$Z \propto \lim_{N \to \infty} \int d\{\mathbf{R}, \mathbf{P}\} e^{-\beta_N H_{rp}(\{\mathbf{R}, \mathbf{P}\})}, \qquad 32.$$

where the ring polymer Hamiltonian is previously defined in Equation 19. Molecular dynamics trajectories generated by this Hamiltonian,

$$\dot{\mathbf{R}}_\alpha = \frac{\partial H_{rp}}{\partial \mathbf{P}_\alpha} \quad \text{and} \quad \dot{\mathbf{P}}_\alpha = -\frac{\partial H_{rp}}{\partial \mathbf{R}_\alpha}, \qquad 33.$$

sample the canonical ensemble and are used in standard PIMD simulations to compute exact thermal equilibrium average properties (78).

RPMD uses these same molecular dynamics trajectories to approximate the real-time, Kubo-transform correlation function (see the sidebar titled Kubo-Transform Correlation Functions) as

$$C_{AB}^{rp}(t) = \frac{1}{Z} \int d\{\mathbf{R}, \mathbf{P}\} e^{-\beta H_{rp}} \overline{A}(\{\mathbf{R(0)}\}, \{\mathbf{P(0)}\}) \overline{B}(\{\mathbf{R(t)}\}, \{\mathbf{P(t)}\}), \qquad 34.$$

where $\overline{O} = \sum_{\alpha=1}^{N} O(\mathbf{P}_\alpha, \mathbf{R}_\alpha)$ are the bead-averaged values of the corresponding operator, and the time-evolved positions and momenta are obtained by integrating the classical equations of motion in Equation 33.

The RPMD approach offers some key advantages over other classical trajectory-based approaches for condensed-phase quantum dynamics. First, the dynamics, by construction, conserve the quantum Boltzmann distribution. This feature ensures that, despite the use of classical trajectories, RPMD simulations do not suffer from unphysical zero-point energy leakage, a common difficulty in semiclassical MV methods (13, 84–86). Second, the ring polymer transition state, as defined by RPMD rate theory, has been shown to emerge naturally as the $t \to 0_+$ limit of the generalized Kubo-transform flux-side correlation function (87–89). Finally, as reviewed elsewhere (41), RPMD and related methods have been remarkably successful in high-dimensional simulations of Born-Oppenheimer dynamics.

2.4.2. Mean-field ring polymer molecular dynamics. As described in Section 2.3.1, tracing over the electronic degrees of freedom yields an MF path-integral expression in nuclear phase space. MF-RPMD (see, for instance, Reference 90), borrowing from the RPMD idea, approximates the real-time Kubo-transform correlation function for a multistate system as

$$C_{AB}^{\text{mf}}(t) = \frac{1}{Z} \int d\{\mathbf{R}, \mathbf{P}\} e^{-\beta H_{\text{mf}}} \text{sgn}(\Theta_{\text{mf}}) \overline{A}(\{\mathbf{R(0)}, \mathbf{P(0)}\}) \overline{B}(\{\mathbf{R(t)}, \mathbf{P(t)}\}), \qquad 35.$$

where $\overline{O}$ indicates the bead-averaged function corresponding to the operator $\hat{O}$, and the time-evolved positions and momenta are obtained by integrating the MF equations of motion defined in Equation 26.

In MF-RPMD, the nuclei evolve in time under an effective state-averaged electronic potential, and the dynamics conserve the quantum Boltzmann distribution. MF-RPMD is practical, easy to implement, and accurate in the strong- to moderate-coupling regimes, but the lack of explicit electronic variables makes these dynamics inaccurate in the nonadiabatic weak-coupling regime.

2.4.3. Mapping variable ring polymer molecular dynamics. The N integrals over electronic positions in Equation 29 can be rewritten as a trace over each of the N electronic variables (50). The trace over an operator can, in turn, be written as a phase-space integral over its Wigner function,

$$\text{Tr}\left[\hat{\mathcal{P}} e^{-\beta_N \mathbf{V}_e(\mathbf{R}_\alpha)} \hat{\mathcal{P}} \right] = \int d\mathbf{x}_\alpha \int d\mathbf{p}_\alpha \int d\mathbf{\Delta x}_\alpha \, e^{i\mathbf{p}_\alpha \cdot \mathbf{\Delta x}_\alpha} \left\langle \mathbf{x}_\alpha + \frac{\mathbf{\Delta x}_\alpha}{2} \middle| \hat{\mathcal{P}} e^{-\beta_N \mathbf{V}_e(\mathbf{R}_\alpha)} \hat{\mathcal{P}} \middle| \mathbf{x}_\alpha - \frac{\mathbf{\Delta x}_\alpha}{2} \right\rangle. \quad 36.$$

Including a single projection operator in Equation 36 is sufficient to constrain the electronic MVs to the SEO subspace but inserting a pair of projection operators symmetrically about the potential operator enables analytic evaluation of the Wigner transform. The resulting expression for the electronic integral is (50)

$$I_{\text{el}}(\{\mathbf{R}\}) = \int d\{\mathbf{x}, \mathbf{p}\}\, e^{-\sum_{\alpha=1}^{N}(\mathbf{x}_\alpha \cdot \mathbf{x}_\alpha + \mathbf{p}_\alpha \cdot \mathbf{p}_\alpha)} \prod_{\alpha=1}^{N}\left(\mathbf{C}_\alpha - \frac{\mathbb{I}}{2}\right)\mathbf{\Gamma}(\mathbf{R}_\alpha),$$ 37.

where $\mathbb{I}$ is the $K \times K$ identity matrix, and the complex electronic matrix is

$$\mathbf{C}_\alpha = (\mathbf{x}_\alpha + i\mathbf{p}_\alpha) \otimes (\mathbf{x}_\alpha - i\mathbf{p}_\alpha)^T.$$ 38.

Inserting the electronic integral back into the expression for canonical partition function in Equation 18 yields an exact, classically isomorphic, phase-space integral in the nuclear degrees of freedom and the electronic MVs,

$$Z \propto \lim_{N\to\infty} \int d\{\mathbf{R}, \mathbf{P}\} \int d\{\mathbf{x}, \mathbf{p}\}\, e^{-\beta_N H_{\text{mv}}} e^{-\sum_{\alpha=1}^{N}(\mathbf{x}_\alpha \cdot \mathbf{x}_\alpha + \mathbf{p}_\alpha \cdot \mathbf{p}_\alpha)} \text{sgn}(\Theta_{\text{mv}}),$$ 39.

where the MV Hamiltonian is

$$H_{\text{mv}} = H_{\text{rp}}(\{\mathbf{R}, \mathbf{P}\}) - \frac{1}{\beta_N}\ln(|\Theta_{\text{mv}}|),$$ 40.

with the ring polymer Hamiltonian, H_{rp}, defined in Equation 19, and the interaction term defined as

$$\Theta_{\text{mv}} = \text{Re}\left\{\text{Tr}\left[\prod_{\alpha=1}^{N}\left(\mathbf{C}_\alpha - \frac{\mathbb{I}}{2}\right)\mathbf{\Gamma}(\mathbf{R}_\alpha)\right]\right\}.$$ 41.

Because Θ_{mv} is not necessarily positive, the absolute value is used in Equation 40, and the corresponding sign function is included in Equation 39; in Equation 41, the real part of the product of complex matrices, $\mathbf{C}_\alpha$, is used, as the canonical partition function and the Kubo-transform correlation function are real valued.

The MV-RPMD approximation to the multistate Kubo-transform correlation functions can then be written as

$$C_{AB}^{\text{mv}}(t) = \frac{1}{Z}\lim_{N\to\infty} \int d\{\mathbf{R}, \mathbf{P}\} \int d\{\mathbf{x}, \mathbf{p}\} e^{-\beta_N H_{\text{mv}}} e^{-\sum_{\alpha=1}^{N}(\mathbf{x}_\alpha \cdot \mathbf{x}_\alpha + \mathbf{p}_\alpha \cdot \mathbf{p}_\alpha)} \text{sgn}(\Theta_{\text{mv}})$$
$$\overline{A}\left[\{\mathbf{R}, \mathbf{P}, \mathbf{x}, \mathbf{p}\}(0)\right]\overline{B}\left[\{\mathbf{R}, \mathbf{P}, \mathbf{x}, \mathbf{p}\}(t)\right],$$ 42.

where the time-evolved positions and momenta are generated by the MV ring polymer Hamiltonian in Equation 40 and the bead-averaged functions $\overline{O} = \sum_{\alpha=1}^{N} O(\mathbf{R}_\alpha)$. The sign function, $\text{sgn}(\Theta_{\text{mv}})$, in Equation 42 and the exponential of $\sum_{\alpha=1}^{N}(\mathbf{x}_\alpha \cdot \mathbf{x}_\alpha + \mathbf{p}_\alpha \cdot \mathbf{p}_\alpha)$ are constants of motion (50, 54) that weight the contribution of each trajectory at $t = 0$. Like RPMD, MV-RPMD trajectories conserve the quantum Boltzmann distribution, and for dynamics on a single electronic surface, the MV-RPMD Hamiltonian simplifies to the RPMD Hamiltonian.

2.4.4. Alternate multistate ring polymer molecular dynamics methods.
Rather than the projected position space identity in Equation 27, an identity in momentum states or even coherent states can be defined to arrive at different but formally exact, classically isomorphic representations of the canonical partition function. The alternate multistate RPMD methods for approximate dynamics differ both in the formulation of the initial thermal distribution and in the Hamiltonian used to generate trajectories in real time. For a quick comparison of multistate RPMD methods, see the sidebar titled Summarizing the Features of MV-RPMD, NRPMD, and CS-RPMD.

SUMMARIZING THE FEATURES OF MV-RPMD, NRPMD, AND CS-RPMD

At $t = 0$, the MV-RPMD correlation function corresponds to the exact Kubo-transform correlation function for linear operators. In the adiabatic limit, at which nuclear dynamics occurs on a single electronic surface, all three approximations reduce to RPMD. Integrating out the electronic variables analytically in all three cases yields MF-RPMD (79).

The MV-RPMD Hamiltonian generates an ensemble of classical trajectories that conserve the quantum Boltzmann distribution (50, 54). The trajectories generated by the MMST-like Hamiltonians in NRPMD and CS-RPMD, like nonadiabatic LSC-IVR (19), fail to conserve the quantum Boltzmann distribution. This failure can lead to zero-point energy leakage, and an inverted potential problem in which the electronic potential takes on negative values (13, 84, 85).

For a bare two-level system with no coupled nuclear degrees of freedom, MV-RPMD fails to capture Rabi oscillations. As one might expect from the success of LSC-IVR for bare two-level systems (19, 79), both NRPMD and CS-RPMD do successfully capture Rabi oscillations (55, 59). In the limiting case of a single ring polymer bead, $N = 1$, the MV-RPMD and NRPMD Hamiltonians are identical and, like CS-RPMD, capture Rabi oscillations and conserve the classical MMST Boltzmann distribution.

2.4.4.1. Nonadiabatic ring polymer molecular dynamics. Path-integral discretization of the Boltzmann operator in electronic variables can be performed by introducing $N/2$ copies of the projected position space identity in Equation 27 and $N/2$ copies of a projected momentum space identity. Analytic evaluation of the resulting electronic matrix elements yields an exact, phase-space expression for the canonical partition function (55),

$$Z \propto \lim_{N \to \infty} \int d\{\mathbf{R}, \mathbf{P}\} \int d\{\mathbf{x}, \mathbf{p}\} \, e^{-\beta_N H_{\mathrm{rp}}} e^{-\left(\sum_{\alpha=1}^{N} \mathbf{x}_\alpha \cdot \mathbf{x}_\alpha + \mathbf{p}_\alpha \cdot \mathbf{p}_\alpha\right)} \Theta_{\mathrm{nr}}, \qquad 43.$$

where

$$\Theta_{\mathrm{nr}} = \mathrm{Tr}\left\{\prod_{\alpha=1}^{N} \left[\mathbf{p}_{\alpha-1}^T \boldsymbol{\Gamma}(R_\alpha) \mathbf{x}_\alpha\right]\left[\mathbf{x}_\alpha^T \boldsymbol{\Gamma}(R_\alpha) \mathbf{p}_\alpha\right]\right\}, \qquad 44.$$

and the matrix $\boldsymbol{\Gamma}$ is defined in Equation 21.

The proposed NRPMD approximation to the Kubo-transform correlation function is (55)

$$C_{AB}^{\mathrm{nr}}(t) = \frac{1}{Z} \lim_{N \to \infty} \int d\{\mathbf{R}, \mathbf{P}\} \int d\{\mathbf{x}, \mathbf{p}\} e^{-\beta_N H_{\mathrm{rp}}} e^{-\left(\sum_{\alpha=1}^{N} \mathbf{x}_\alpha \cdot \mathbf{x}_\alpha + \mathbf{p}_\alpha \cdot \mathbf{p}_\alpha\right)} \Theta_{\mathrm{nr}}$$
$$\overline{A}\left[\{\mathbf{R}, \mathbf{P}, \mathbf{x}, \mathbf{p}\}(0)\right] \overline{B}\left[\{\mathbf{R}, \mathbf{P}, \mathbf{x}, \mathbf{p}\}(t)\right], \qquad 45.$$

where $\overline{A}$ and $\overline{B}$ are bead-averaged functions, and the time-evolved positions and momenta are obtained by integrating equations of motion generated by a different Hamiltonian,

$$H_{\mathrm{nr}} = H_{\mathrm{rp}}(\{R, P\}) + \frac{1}{2}\sum_{\alpha=1}^{N}\left(\mathbf{x}_\alpha^T \mathbf{V}_e \mathbf{x}_\alpha + \mathbf{p}_\alpha^T \mathbf{V}_e \mathbf{p}_\alpha - \mathrm{Tr}\,[\mathbf{V}_e]\right). \qquad 46.$$

Equations of motion for the electronic mapping variables under the NRPMD Hamiltonian in Equation 46 describe each bead evolving under the semiclassical MMST Hamiltonian previously defined in Equation 12. However, unlike MV-RPMD, the classical trajectory ensemble used here does not conserve the quantum Boltzmann distribution.

2.4.4.2. Coherent-state ring polymer molecular dynamics.

As the name suggests, CS-RPMD is derived by inserting identity in the form of an overcomplete set of coherent states (59). Evaluating the electronic integral then yields an expression that is exact in the $N \to \infty$ limit,

$$Z \propto \lim_{N \to \infty} \int d\{\mathbf{R}, \mathbf{P}\} \int d\{\mathbf{x}, \mathbf{p}\} e^{-\beta_N H_{cs}} \Theta_{cs}, \qquad 47.$$

where the CS-RPMD Hamiltonian is

$$H_{cs} = H_{rp} + \sum_{\alpha=1}^{N} \frac{1}{2} \left(\mathbf{x}_\alpha^T \mathbf{V}_e \mathbf{x}_\alpha + \mathbf{p}_\alpha^T \mathbf{V}_e \mathbf{p}_\alpha \right) - \text{Tr}\left[\mathbf{V}_e\right] \qquad 48.$$

with the interaction term

$$\Theta_{cs} = e^{-\sum_\alpha (\mathbf{x}_\alpha \cdot \mathbf{x}_\alpha + \mathbf{p}_\alpha \cdot \mathbf{p}_\alpha)} \text{Tr}\left[\prod_{\alpha=1}^{N} \frac{1}{2} (\mathbf{x}_\alpha + \mathbf{p}_\alpha) \otimes (\mathbf{x}_\alpha - i\mathbf{p}_\alpha)^T \right]. \qquad 49.$$

CS-RPMD approximates the Kubo-transform correlation function as

$$C_{AB}^{cs}(t) = \frac{1}{Z} \int d\{\mathbf{R}, \mathbf{P}\} \int d\{\mathbf{x}, \mathbf{p}\} e^{-\beta_N H_{cs}} \Theta_{cs}$$
$$\overline{A}\left[\{\mathbf{R}, \mathbf{P}, \mathbf{x}, \mathbf{p}\}(0)\right] \overline{B}\left[\{\mathbf{R}, \mathbf{P}, \mathbf{x}, \mathbf{p}\}(t)\right], \qquad 50.$$

where the time-evolved positions and momenta are generated by the CS-RPMD Hamiltonian in Equation 48. Unfortunately, CS-RPMD trajectories also fail to conserve the quantum Boltzmann distribution, because Θ_{cs} is not a constant of motion.

2.5. Exact Quantum Liouvillian in the Mapping-Variable Representation

Deriving an exact ring polymer Liouvillian for quantum dynamics in the MV framework is a step toward the rigorous derivation of approximate real-time, multistate RPMD methods. For adiabatic dynamics, it has been shown that RPMD and CMD can both be connected to an exact quantum Liouvillian derived from a generalized Kubo-transform correlation function that is equivalent to the Kubo-transform correlation function for bead-invariant operators and in the $N \to \infty$ limit (87, 88, 91).

An analytic expression for the exact N-bead, path-integral Liouvillian in the phase space of the nuclear and electronic degrees of freedom can be similarly derived (92):

$$\mathcal{L}^{[N]} = \mathcal{L}_{\text{nuc}}^{[N]} + \mathcal{L}_{\text{elec}}^{[N]} + \mathcal{L}_{\text{hd}}^{[N]}, \qquad 51.$$

where the first term corresponds to nuclear evolution on an Ehrenfest-like average electronic surface,

$$\mathcal{L}_{\text{nuc}}^{[N]} = \sum_{\alpha=1}^{N} \mathbf{P}_\alpha^T \mathbf{M}^{-1} \frac{\partial}{\partial \mathbf{R}_\alpha} - \frac{2}{\hbar} \left[V_0(\mathbf{R}_\alpha) + V_{\text{sc}}(\mathbf{R}_\alpha, \mathbf{x}_\alpha, \mathbf{p}_\alpha) \right] \sin\left(\frac{\hbar}{2} \frac{\overleftarrow{\partial}}{\partial \mathbf{R}_\alpha} \frac{\overrightarrow{\partial}}{\partial \mathbf{P}_\alpha} \right), \qquad 52.$$

the second term describes the Rabi oscillations of the electronic degrees of freedom along with higher-order couplings to nuclear derivatives,

$$\mathcal{L}_{\text{elec}}^{[N]} = \sum_{\alpha=1}^{N} \frac{1}{\hbar} \left[\mathbf{p}_\alpha \mathbf{V}_e(\mathbf{R}_\alpha) \overrightarrow{\nabla_{\mathbf{x}_\alpha}} - \mathbf{x}_\alpha \mathbf{V}_e(\mathbf{R}_\alpha) \overrightarrow{\nabla_{\mathbf{p}_\alpha}} \right] \cos\left(\frac{\hbar}{2} \frac{\overleftarrow{\partial}}{\partial \mathbf{R}_\alpha} \frac{\overrightarrow{\partial}}{\partial \mathbf{P}_\alpha} \right), \qquad 53.$$

and the third term corresponds to nuclear and electronic evolution due to higher-order derivatives in both degrees of freedom,

$$\mathcal{L}_{\text{hd}}^{[N]} = \sum_{\alpha=1}^{N} \frac{1}{4} \left[\overrightarrow{\nabla_{\mathbf{x}_\alpha}} \mathbf{V}_e(\mathbf{R}_\alpha) \overrightarrow{\nabla_{\mathbf{x}_\alpha}} + \overrightarrow{\nabla_{\mathbf{p}_\alpha}} \mathbf{V}_e(\mathbf{R}_\alpha) \overrightarrow{\nabla_{\mathbf{p}_\alpha}} \right] \sin\left(\frac{\hbar}{2} \frac{\overleftarrow{\partial}}{\partial \mathbf{R}_\alpha} \frac{\overrightarrow{\partial}}{\partial \mathbf{P}_\alpha} \right). \qquad 54.$$

MATSUBARA APPROXIMATION

A complex Matsubara Liouvillian for adiabatic dynamics can be derived by rewriting the exact ring polymer Liouvillian in terms of the N normal modes of a free ring polymer and then truncating to include only $M < N$ smooth or Matsubara modes (87). The resulting complex Liouvillian preserves the quantum Boltzmann distribution, and the real part describes dynamics under the RPMD Hamiltonian (87, 88, 91, 93).

Starting with the exact multistate ring polymer Liouvillian (92), transforming to the normal modes of the free nuclear ring polymer, and truncating to include only $M < N$ normal modes yield a complex multistate Matsubara Liouvillian (58). Unlike the adiabatic case, this multistate Liouvillian does not conserve the quantum Boltzmann distribution for a general K-level system. The real part of this multistate Matsubara Liouvillian gives rise to dynamics in the hybrid MS-RPMD framework outlined in Section 2.5 (58).

In Equation 52, V_{sc} is the MMST potential (last term in Equation 12) and the arrows over the F-dimensional nuclear partial derivatives indicate the direction in which the derivative is evaluated. In Equation 53, $\mathbf{V}_e$ is the diabatic potential energy matrix and $\nabla_{\mathbf{x/p}}$ indicate partial derivatives with respect to the K-dimensional vectors of electronic position or momentum MVs, respectively.

Interestingly, all three terms in the Liouvillian describe a ring polymer dynamics in which each bead evolves independently in time. The beads are, however, connected to each other at time $t = 0$ through the initial thermal distribution that resembles the MV-RPMD distribution for the electron degrees of freedom but includes an additional nontrivial Wigner transform in the nuclear degrees of freedom (92). Constructing an approximate classical ring polymer Hamiltonian for multistate system dynamics requires that the exact quantum Liouvillian be truncated to eliminate higher-order derivatives.

Truncating $\mathcal{L}^{[N]}$ to $\mathcal{O}(\hbar^0)$ results in classical dynamics that do not conserve the quantum Boltzmann distribution:

$$\mathcal{L}_0^{[N]} = \sum_{\alpha=1}^{N} \mathbf{P}_\alpha^T \mathbf{M}^{-1} \frac{\partial}{\partial \mathbf{R}_\alpha} - \left[V_0\left(\mathbf{R}_\alpha\right) + V_{sc}\left(\mathbf{R}_\alpha, x_\alpha, \mathbf{p}_\alpha\right) \right] \overleftarrow{\frac{\partial}{\partial \mathbf{R}_\alpha}} \overrightarrow{\frac{\partial}{\partial \mathbf{P}_\alpha}} \qquad 55.$$

$$+ \frac{1}{\hbar}\left[\mathbf{p}_\alpha \mathbf{V}_e\left(\mathbf{R}_\alpha\right) \overrightarrow{\nabla_{\mathbf{x}_\alpha}} - \mathbf{x}_\alpha \mathbf{V}_e\left(\mathbf{R}_\alpha\right) \overrightarrow{\nabla_{\mathbf{p}_\alpha}} \right]. \qquad 56.$$

This truncated Liouvillian suggests a hybrid MS-RPMD scheme with trajectories initialized from an MV-RPMD distribution and time evolved under the NRPMD Hamiltonian. For more details, please see the sidebar titled Matsubara Approximation.

3. IMPLEMENTATION

All calculations using the imaginary-time, path-integral-based methods discussed here are converged in the limit $N \rightarrow \infty$. Multistate RPMD methods are expected to converge with relatively low N values for nonadiabatic system simulations, as the number of beads depends on temperature and the magnitude of the electronic coupling.

3.1. Thermal Correlation Functions

Approximate multistate RPMD thermal correlation functions take the form

$$C_{AB}^{ms}(t) = \frac{\langle A(\{\mathbf{x_0}, \mathbf{p_0}, \mathbf{R_0}, \mathbf{P_0}\}) B(\{\mathbf{x_t}, \mathbf{p_t}, \mathbf{R_t}, \mathbf{P_t}\}) Q(\{\mathbf{x_0}, \mathbf{p_0}, \mathbf{R_0}, \mathbf{P_0}\}) \rangle_{\mathbf{W}}}{\langle Q(\{\mathbf{x_0}, \mathbf{p_0}, \mathbf{R_0}, \mathbf{P_0}\}) \rangle_{\mathbf{W}}}, \qquad 57.$$

Table 1 Implementation details for MV-RPMD, NRPMD, and CS-RPMD

Method	W	Sampling	Q	H_{ms}
MV-RPMD	$e^{-\beta H_{mv}} e^{-\sum_{\alpha=1}^{N}(\mathbf{x}_\alpha \cdot \mathbf{x}_\alpha + \mathbf{p}_\alpha \cdot \mathbf{p}_\alpha)}$	PIMC	$\mathrm{sgn}(\Theta_{mv})^a$	$H_{mv}{}^b$
NRPMD	$e^{-\beta H_{rp}} e^{-\sum_{\alpha=1}^{N}(\mathbf{x}_\alpha \cdot \mathbf{x}_\alpha + \mathbf{p}_\alpha \cdot \mathbf{p}_\alpha)} |\Theta_{nr}|$	PIMC	$\mathrm{sgn}(\Theta_{nr})^c$	$H_{nr}{}^d$
CS-RPMD	$e^{-\beta H_{cs}}$	PIMD	$\Theta_{cs}{}^e$	$H_{cs}{}^f$
Hybrid MS-RPMD^g	$e^{-\beta H_{mv}} e^{-\sum_{\alpha=1}^{N}(\mathbf{x}_\alpha \cdot \mathbf{x}_\alpha + \mathbf{p}_\alpha \cdot \mathbf{p}_\alpha)}$	PIMC	$\mathrm{sgn}(\Theta_{mv})$	H_{nr}

Abbreviations: CS-RPMD, coherent-state ring polymer molecular dynamics; MS-RPMD, multistate ring polymer molecular dynamics; MV-RPMD, mapping-variable ring polymer molecular dynamics; NRPMD, nonadiabatic ring polymer molecular dynamics; PIMC, path-integral Monte Carlo; PIMD, path-integral molecular dynamics.
[a]Equation 41.
[b]Equation 40.
[c]Equation 44.
[d]Equation 46.
[e]Equation 49.
[f]Equation 48.
[g]Hybrid multistate RPMD from nonadiabatic Matsubara derivation (58).

where ms = {mv, nr, cs}, the subscripts **0** and **t** indicate the initial or time-evolved phase-space vectors, respectively, and the notation $\langle \cdot \rangle_W$ is used to indicate a thermal ensemble average over a distribution W. Trajectory initial conditions are generated from the distribution W using standard PIMC or PIMD methods, and then time-evolved by integrating Hamilton's equation of motion for a multistate Hamiltonian.

The forms of the distribution W and the Hamiltonian H_{ms} used to generate real-time trajectories for each of the approximate multistate RPMD methods described here are specified in **Table 1**.

The function Q that appears in the denominator of Equation 57 is the estimator for the canonical partition function such that

$$ Z = \lim_{N \to \infty} \int d\{\mathbf{R}, \mathbf{P}\} \int d\{\mathbf{x}, \mathbf{p}\} Q(\mathbf{x}, \mathbf{p}, \mathbf{R}, \mathbf{P}) W(\mathbf{x}, \mathbf{p}, \mathbf{R}, \mathbf{P}). \qquad 58. $$

For single-surface, Born-Oppenheimer processes, $Q = 1$, but for multistate systems, this function accounts for the fact that the isomorphic classical expression for the canonical partition function does not, in general, correspond to a positive definite distribution.

3.2. Estimators

The functions A and B in the numerator of Equation 57 are estimators derived to yield the exact thermal equilibrium average values, $\langle \hat{A} \rangle$ and $\langle \hat{B} \rangle$, when the trajectory ensemble is sampled from the function W. Detailed derivations are not presented here, but some of the estimators most frequently used in the multistate RPMD methods are introduced.

When the operators depend on nuclear position $O(\hat{\mathbf{R}})$, the corresponding bead-averaged estimators are $O(\{\mathbf{R}\}) = 1/N \sum_{\alpha=1}^{N} O(\mathbf{R}_\alpha)$. For electronic state population operators, several estimators have been derived and shown to be exact for the calculation of thermal equilibrium properties. Specifically, three estimators have been derived for the electronic state projection operator $\mathcal{P}_n = |n\rangle\langle n|$ in the MV-RPMD framework. The Boltzmann population estimator takes the form (50)

$$ \mathcal{P}_n^\beta = \frac{[\Theta_{mv}]_{nn}}{\mathrm{Tr}[\Theta_{mv}]}, \qquad 59. $$

where the matrix Θ_{mv} is defined in Equation 41, and the notation $[.]_{nn}$ is used to indicate the corresponding matrix element. The Wigner estimator has been used in the simulation of photoinitiated, excited-state dynamics (51),

$$\mathcal{P}_n^W = \frac{2^{K+1}}{N} \sum_{\alpha=1}^{N} e^{-\sum_\alpha \mathbf{x}_\alpha \cdot \mathbf{x}_\alpha + \mathbf{p}_\alpha \cdot \mathbf{p}_\alpha} \left([\mathbf{x}_\alpha]_n^2 + [\mathbf{p}_\alpha]_n^2 - \frac{\hbar}{2} \right).$$

60.

The semiclassical estimator was first introduced as a population estimator in the NRPMD framework but was subsequently shown to be exact in the MV-RPMD framework as well (52, 55):

$$\mathcal{P}_n^{sc} = \frac{1}{2N} \sum_{\alpha=1}^{N} \left([\mathbf{x}_\alpha]_n^2 + [\mathbf{p}_\alpha]_n^2 - \hbar \right).$$

61.

Finally, in the CS-RPMD framework, the population estimator takes the form

$$\mathcal{P}_n^{cs} = \frac{1}{N} \sum_{\alpha=1}^{N} \frac{[\mathbf{x}_\alpha - i\mathbf{p}_\alpha]_n [\mathbf{x}_{\alpha+1} + i\mathbf{p}_{\alpha+1}]_n}{(\mathbf{x}_\alpha - i\mathbf{p}_\alpha)^T (\mathbf{x}_{\alpha+1} + i\mathbf{p}_{\alpha+1})}.$$

62.

3.3. Nonequilibrium Correlation Functions

The short-time accuracy of RPMD for nonequilibrium correlation functions has been established through connections with Matsubara dynamics and demonstrated through numerical simulations (94). Although the short-time accuracy of the multistate RPMD methods has not been clearly established, recent work developing a nonadiabatic Matsubara dynamics suggests that their performance is likely similar for thermal equilibrium correlation functions and nonequilibrium correlation functions (58).

The protocol for initializing to a photoinduced excited state was developed in the context of the MV-RPMD framework (51) and later adapted to an NRPMD implementation as well (59). Assuming vertical Franck-Condon excitation, nuclear phase-space variables can be initialized from a ground-state equilibrium distribution. Initial conditions for electronic MVs are then chosen such that only one electronic state is initially populated. Drawing on ideas from the semiclassical literature (95), this can be achieved by setting the Wigner or the semiclassical population estimators (Equations 60 and 61) for each bead to 0 for an unpopulated state, 1 for a fully populated state, or a number between 0 and 1 for partially populated states.

It is necessary to determine a dynamical temperature, as the multistate RPMD Hamiltonian depends on the inverse temperature, $\beta = 1/k_B T$. For a thermal simulation, β is determined by the physical temperature of the simulation. However, for a system initially in the excited state, a fictitious dynamical temperature, T_d, is necessary to account for the excess energy introduced to the system upon photoexcitation. Numerical simulations demonstrate that the best choice of fictitious temperature is $T_d k_B = E_i$, where k_B is the Boltzmann constant and E_i is the total initial energy of the system in the excited state (51).

4. APPLICATIONS

Multistate RPMD methods have been used in a range of applications including vibronic spectra calculations (56), dynamic simulations of spin-boson models (50, 54, 55, 59) and photoinduced excited-state dynamics (51, 57), and in studies of proton-coupled electron transfer (52). In this section, I discuss three specific studies that highlight the strengths of these approaches.

4.1. Two-Level Systems

Approximate multistate RPMD methods are benchmarked through the study of two-level systems coupled to a single nuclear degree of freedom. Nuclear dynamics is characterized through calculations of the nuclear position autocorrelation function, where $\hat{A} = \hat{B} = \hat{R}$.

In the adiabatic (strong-coupling) regime, both the MF-RPMD and MV-RPMD nuclear autocorrelation functions agree well with exact quantum results, as shown in **Figure 1a**. As the coupling strength is decreased and nonadiabatic effects start to play a significant role, MV-RPMD outperforms MF-RPMD, as shown in **Figure 1b–d**. While not shown here, it has been established that, despite minor differences in the nuclear autocorrelation function calculated using MV-RPMD, CS-RPMD, and NRPMD for these systems, there is little to choose between them in
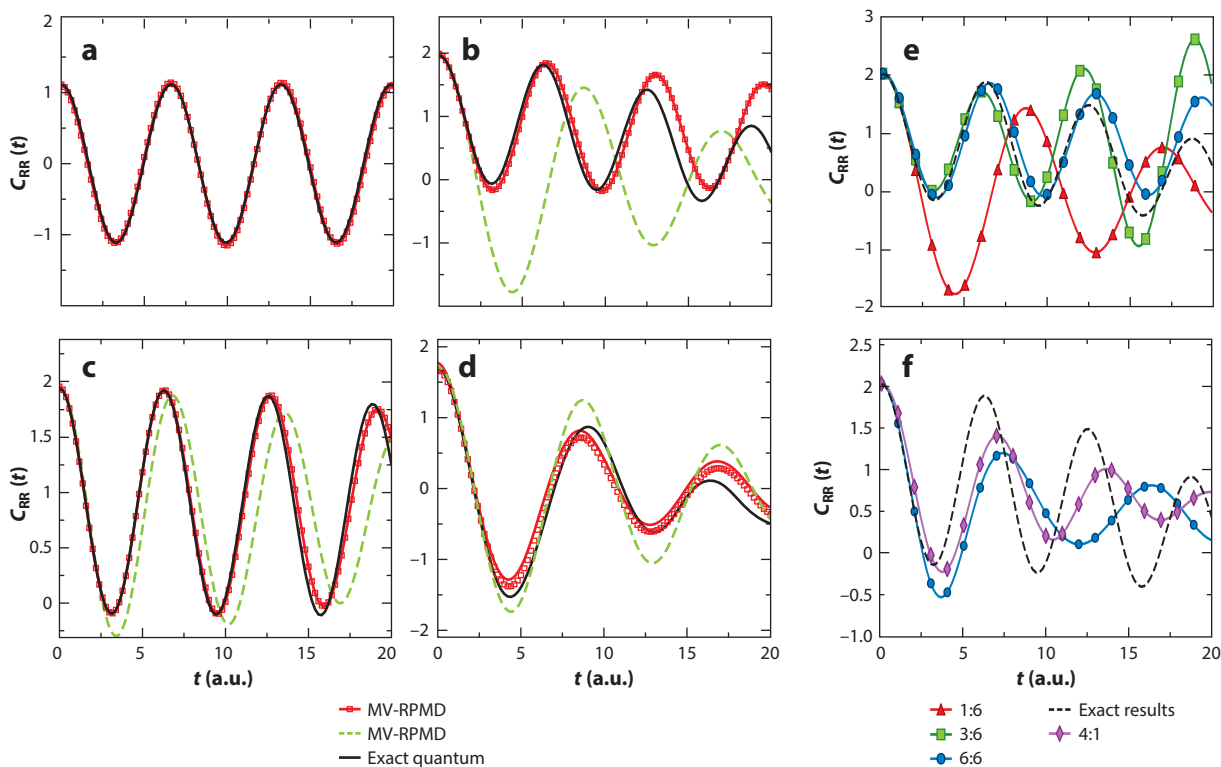

Figure 1

The mapping-variable ring polymer molecular dynamics (MV-RPMD) nuclear autocorrelation functions, $C_{RR}(t)$, for a two-level system coupled to a single nuclear mode are calculated using Equation 42 with $A = B = \bar{R}$. The converged number of beads ranges from $N = 5$ in the weak- and moderate-coupling regimes to $N = 10$ in the strong-coupling case. The number of trajectories required goes from 10^4 to 10^5, with the larger number corresponding to stronger coupling and more beads. The diagonal elements of the diabatic potential energy matrix are shifted oscillators, and the off-diagonal coupling is tuned from (*a*) the adiabatic, strong-coupling regime to (*b*) moderate coupling to (*c*) the nonadiabatic, weak-coupling regime with nonzero driving force and (*d*) a symmetric nonadiabatic coupling model. MV-RPMD results are plotted using red lines with squares and mean-field (MF)-RPMD results are shown as green dashed lines. Exact quantum results, generated by diagonalizing a discrete-variable representation Hamiltonian on a grid (96), are shown with solid black lines. Panels *a–d* adapted from Reference 50. (*e,f*) These graphs explore mixed time slicing for the model system in panel *d*, in which different numbers of beads are used to discretize the electronic N_e and nuclear degrees of freedom N_n. Panel *e* plots the nuclear position autocorrelation function with $N_e:N_n$ values 1:6 with red triangles, 3:6 with green squares, 6:6 with blue circles, and exact results with black dashed lines. Panel *f* plots the nuclear autocorrelation function with more beads for the electronic state variable, representing the function with $N_e:N_n$ values 4:1 with purple diamonds. Panels *e* and *f* adapted from Reference 54.

terms of accuracy (59). Furthermore, a recent study (97) on the use of mixed time slicing with MV-RPMD in which different numbers of beads are used to describe the electronic and nuclear degrees of freedom suggests that when nuclear and electronic motion are strongly coupled, the best results are obtained by quantizing them to the same extent, as demonstrated in **Figure 1e,f** (54).

Both NRPMD and CS-RPMD have been used to compute electronic state population correlation functions for these same model systems and find good agreement with exact quantum results (57, 59). Expectedly, these results closely resemble those generated by LSC-IVR calculations in which the Wigner transform of the Boltzmann operator is obtained from an exact calculation (79). However, MV-RPMD population autocorrelation functions are noisy and deviate rapidly from the exact result even at relatively short times.

4.2. Excited-State Dynamics

The different mechanisms of ultrafast photoinduced dissociation can be modeled using a manifold of three coupled excited states, where one is initially occupied through photoexcitation. Coronado et al.'s study (98) considers three model systems that differ in the relative timescales on which branching events are observed and in the extent of coupling between the different excited-state surfaces.

Figure 2a demonstrates that the time-dependent electronic state populations calculated in an MV-RPMD simulation capture the short-time behavior for all three model systems. However, at longer times, MV-RPMD proves less accurate, particularly for the first model, in which the two curve-crossing events are well separated in time. Results for the same models from an NRPMD simulation are shown in **Figure 2b**. It is evident that these dynamics are more accurate at longer times, in particular even capturing the longer timescale transitions in the first model system. Interestingly, MV-RPMD simulations in the classical one-bead limit are comparably accurate with NRPMD, as shown in **Figure 2c**, because the MV-RPMD Hamiltonian reduces to the NRPMD Hamiltonian for dynamics in this limit.

4.3. Mechanistic Study of Proton-Coupled Electron Transfer

Proton-coupled, electron-transfer (PCET) reactions are a class of reactions that are central to understanding important chemical processes such as water-splitting catalysis, bioinorganic reactions, and enzyme catalysis. PCET can be theoretically described using a system-bath model (2) in which four electron–proton diabatic states are coupled to solvent degrees of freedom that are, in turn, coupled to a thermal bath representing the environment. The four electron–proton states are quasi-diabatic states labeled DD, DA, AD, and AA, where the first and second letters indicate the electron or proton is in its donor (D) or acceptor (A) state, respectively. The mechanistic study described here focuses on the chronology of charged particle transfer—some systems exhibit concerted electron and proton transfer, while others undergo sequential transfer events with either the electron transferring first (ET-PT mechanism) or the proton transferring first (PT-ET mechanism) (2).

MV-RPMD simulations were recently used to successfully characterize the mechanism of PCET in a series of model systems (52). A nonequilibrium initial distribution was generated by constraining the system to a dividing surface defined by nuclear configurations corresponding to the curve crossing between the reactant (DD) diabatic state and one of the other three diabatic states. Time-evolving trajectories forward and backward in time from this dividing surface served to highlight the different PCET mechanisms. Specifically, following the timescales on which population transfers from the reactant to the other diabatic states yielded mechanistic insight. For instance, **Figure 3** shows the results of an MV-RPMD study of population dynamics for a model
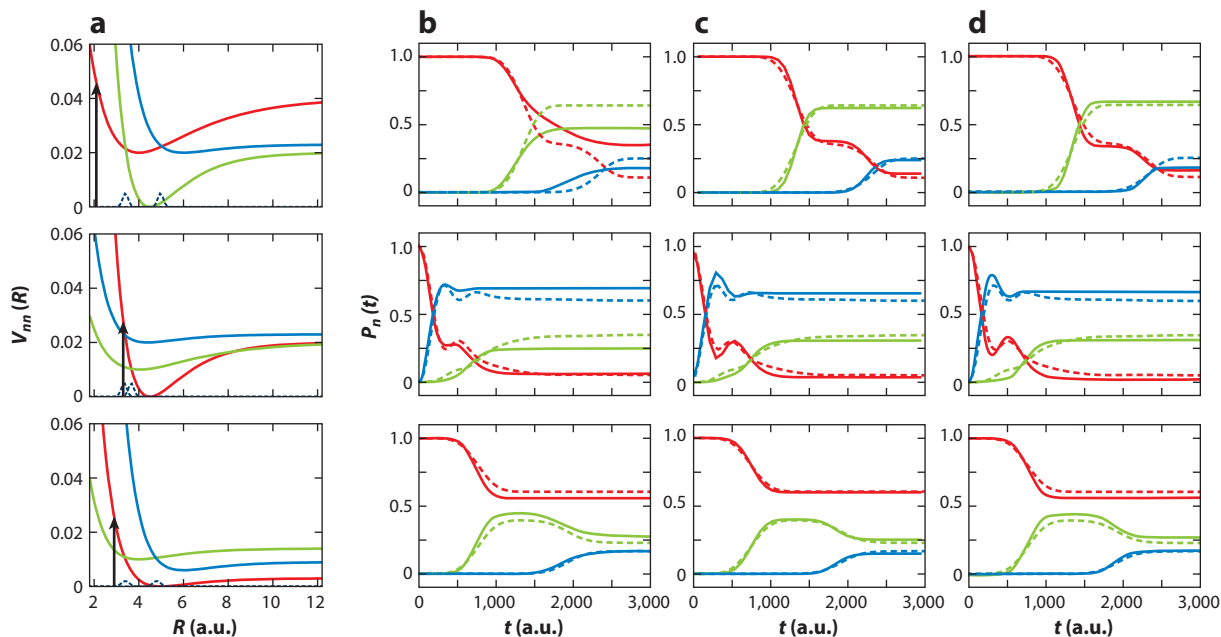
Figure 2

(*a*) Three model systems in which the three coupled, diabatic, excited-state potential energy surfaces, $V_{nn}(R)$, are described by Morse functions and the black arrows indicate the state initially populated upon photoexcitation from the ground state. The excited-state populations, $\mathcal{P}_n(t)$, plotted in panels *b–d* are color coded to match the corresponding potential surfaces in panel *a*. (*b*) Excited-state population dynamics from bead-converged ($N = 4$), mapping-variable ring polymer molecular dynamics (MV-RPMD) calculations using the Wigner estimator (*solid lines*). The number of trajectories employed ranges from 2×10^3 to 3×10^4, with (*top*) model I requiring the fewest trajectories and (*bottom*) model III requiring the most. Exact quantum results are plotted with dashed lines in panels *b–d*. (*c*) Time-dependent populations from nonadiabatic RPMD (NRPMD) using the semiclassical estimator. The plots in panel *c* are made with data provided by the authors of Reference 57. (*d*) MV-RPMD population dynamics in the $N = 1$ classical limit (*solid lines*) that agree remarkably well with NRPMD results. Panels *a*, *b*, and *d* adapted from Reference 51.

system initially constrained to two different dividing surfaces. In both cases, it is evident that, as the population of the reactant (DD) state decreases, the population of the electron-transfer (AD) state increases first, followed by a subsequent transfer of population to the product (AA) state. These studies served as the first demonstration of the utility of multistate RPMD methods in high-dimensional, condensed-phase systems, and further serve to establish dividing surface independence in MV-RPMD simulations of population dynamics (52).

5. LIMITATIONS

5.1. Reaction Rate Theory

The success of RPMD in the calculation of condensed-phase reaction rates has been shown to arise from the connections between RPMD rate theory and the quantum transition-state theory derived from the generalized flux-side, Kubo-transform correlation function (91). The development of a multistate RPMD rate theory is key to enabling large-scale application of these methods and remains an outstanding challenge.

Other multistate methods based on RPMD have had some success in the calculation of rates, such as ring polymer surface hopping (99), kinetically constrained (KC)-RPMD (100, 101), and MF-RPMD for the calculation of adiabatic and nonadiabatic reaction rates in multistate
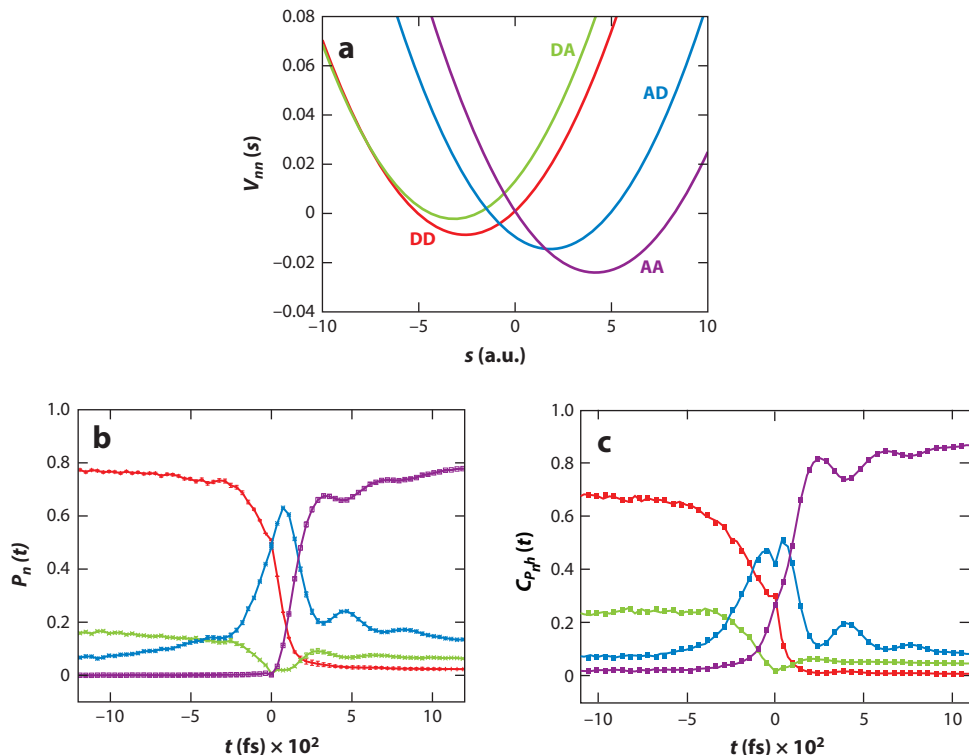
Figure 3

(*a*) The four diabatic potential energy surfaces, $V_{nn}(S)$, labeled DD, DA, AD, and AA for a model PCET system, are pictured. (*b*) A plot showing the change in population, $\mathcal{P}_n(t)$, calculated using the Boltzmann population estimator introduced in Section 3.2, for each of the four diabatic states color coded to match panel *a*. The focusing protocol introduced in Section 3.3 is used to sample the initial electronic MVs such that the semiclassical population estimators for the DD and AD states are equal to 0.5, those for the AD and AA states are equal to 0, and the nuclear position is set to $s = -0.8$ a.u., corresponding to the crossing between the DD and AD diabatic states. Trajectories are run forward and backward in time and spliced together to discover the PCET mechanism; here the population dynamics demonstrate that the PCET is sequential, with ET preceding PT (ET-PT mechanism). (*c*) A plot showing the Boltzmann population dynamics for the same model system obtained from an MV-RPMD simulation in which the initial electronic MVs are sampled such that the semiclassical population estimators for the DD and AA states are equal to 0.5, those for the DA and AD states are equal to 0, and the nuclear position is set to $s = 0$ a.u., corresponding to the crossing between the DD and AA diabatic states. The resulting population changes correctly predict an ET-PT mechanism, demonstrating that dynamics in the MV-RPMD framework are independent of the choice of dividing surface. All calculations are converged with $N = 10$ beads using an ensemble of $\sim 10^5$ classical trajectories. Abbreviations: A, acceptor; D, donor; ET, electron transfer; MV-RPMD, mapping-variable ring polymer molecular dynamics; PCET, proton-coupled electron transfer; PT, proton transfer.

systems (102). KC-RPMD introduces a single auxiliary variable that reports on the probability of electronic transitions and employs trajectories that conserve an approximate quantum Boltzmann distribution in this expanded phase space (100). Nonadiabatic reaction rates calculated in the MF-RPMD framework require the introduction of an ad hoc constraint to ensure that trajectories pass through the electronic transition state (102). In a practical sense, MF-RPMD offers a simple and scalable approach to the calculation of nonadiabatic condensed-phase reaction rates; however, the lack of explicit electronic variables limits mechanistic insights.

Given the importance of dynamics that preserve detailed balance in the context of rate calculations, it is expected that recent work understanding the nature of MV-RPMD dynamics (53, 54, 92) and the derivation of new population estimators (51, 52) will pave the way to developing a rigorous rate theory with explicit electronic variables.

5.2. Detailed Balance and Rabi Oscillations

As discussed in earlier sections, multistate RPMD methods developed to date either conserve the quantum Boltzmann distribution (MV-RPMD) or, like nonadiabatic LSC-IVR, correctly describe the electronic transitions in bare two-level systems (NRPMD and CS-RPMD). The hybrid multistate method derived from the nonadiabatic Matsubara Liouvillian also falls in this latter category, with dynamics that do not obey detailed balance. Deriving an imaginary-time, path-integral-based dynamics that can both capture Rabi oscillations and preserve detailed balance remains an outstanding theoretical challenge.

5.3. Ab Initio Path Integrals for Nonadiabatic Dynamics

Ab initio dynamics refers to trajectory-based simulations in which the potential energy and forces are computed on the fly from electronic structure. Ab initio multistate path-integral dynamics faces additional challenges. First, the Schrödinger equation must be solved for multiple adiabatic eigenvalues and eigenstates at each time step. Second, the multistate methods described here all assume a diabatic electronic Hamiltonian whose diagonal and off-diagonal elements must be obtained from an on-the-fly diabatization. Some promising avenues toward this goal include recent work that proposes circumventing diabatization altogether (103, 104) and advances in the rapid calculation of quasi-diabatic states, briefly referenced in the sidebar titled Adiabatic and Diabatic Representations.

5.4. Borrowing Limitations from Ring Polymer Molecular Dynamics

Multistate RPMD methods are extensions of RPMD to systems in which multiple electronic states are coupled to nuclear degrees of freedom. The limitations of RPMD must, therefore, be taken into account: Specific concerns include the spurious dynamical frequencies introduced by the spring terms between neighboring beads (105), inaccuracies in describing nuclear correlation functions with nonlinear operators (106), and the inability to capture nuclear quantum coherence effects at times $> \beta \hbar$ (44, 46).

6. OUTLOOK

This review introduces readers to the theoretical foundations of the recently developed multistate RPMD methods for the simulation of nonadiabatic reactions in the condensed phase using only classical trajectories in an extended electron–nuclear phase space. The applications discussed here demonstrate the versatility of these multistate path-integral methods, and the availability of open-source software will enable their broader use (107). The many exciting avenues for future research include ab initio multistate path-integral studies and the derivation of a rigorous nonadiabatic reaction rate theory.

DISCLOSURE STATEMENT

The author is not aware of any affiliations, memberships, funding, or financial holdings that might be perceived as affecting the objectivity of this review.

ACKNOWLEDGMENTS

LITERATURE CITED

1. Evans RFL, Fan WJ, Chureemart P, Ostler TA, Ellis MOA, Chantrell RW. 2014. Atomistic spin model simulations of magnetic nanomaterials. *J. Phys. Condens. Matter* 26(10):103202
2. Hammes-Schiffer S. 2001. Theoretical perspectives on proton-coupled electron transfer reactions. *Acc. Chem. Res.* 34(4):273–81
3. Born M, Oppenheimer R. 1927. Zur Quantentheorie der Molekeln [On the quantum theory of molecules]. *Ann. Phys.* 389(20):457–84
4. Makri N, Makarov DE. 1995. Tensor propagator for iterative quantum time evolution of reduced density matrices. II. Numerical methodology. *J. Chem. Phys.* 102(11):4611–18
5. Beck MH, Jäckle A, Worth GA, Meyer HD. 2000. The multiconfiguration time-dependent Hartree (MCTDH) method: a highly efficient algorithm for propagating wavepackets. *Phys. Rep.* 324(1):1–105
6. Wang H, Thoss M. 2003. Multilayer formulation of the multiconfiguration time-dependent Hartree theory. *J. Chem. Phys.* 119(3):1289–99
7. Bonfanti M, Worth GA, Burghardt I. 2020. Multi-configuration time-dependent Hartree methods: from quantum to semiclassical and quantum-classical. In *Quantum Chemistry and Dynamics of Excited States*, ed. L González, R Lindh, pp. 383–411. Hoboken, NJ: Wiley
8. Greene SM, Batista VS. 2017. Tensor-train split-operator Fourier transform (TT-SOFT) method: multidimensional nonadiabatic quantum dynamics. *J. Chem. Theory Comput.* 13(9):4034–42
9. Richings G, Polyak I, Spinlove K, Worth G, Burghardt I, Lasorne B. 2015. Quantum dynamics simulations using Gaussian wavepackets: the vMCG method. *Int. Rev. Phys. Chem.* 34(2):269–308
10. Curchod BF, Martínez TJ. 2018. Ab initio nonadiabatic quantum molecular dynamics. *Chem. Rev.* 118(7):3305–36
11. Meyer HD, Miller WH. 1979. A classical analog for electronic degrees of freedom in nonadiabatic collision processes. *J. Chem. Phys.* 70(7):3214–23
12. Stock G, Thoss M. 1997. Semiclassical description of nonadiabatic quantum dynamics. *Phys. Rev. Lett.* 78(4):578–81
13. Thoss M, Stock G. 1999. Mapping approach to the semiclassical description of nonadiabatic quantum dynamics. *Phys. Rev. A* 59(1):64–79
14. Miller WH. 2001. The semiclassical initial value representation: a potentially practical way for adding quantum effects to classical molecular dynamics simulations. *J. Phys. Chem. A* 105(13):2942–55
15. Sun X, Wang H, Miller WH. 1998. Semiclassical theory of electronically nonadiabatic dynamics: results of a linearized approximation to the initial value representation. *J. Chem. Phys.* 109(17):7064–74
16. Wang H, Sun X, Miller WH. 1998. Semiclassical approximations for the calculation of thermal rate constants for chemical reactions in complex molecular systems. *J. Chem. Phys.* 108(23):9726–36
17. Wang H, Song X, Chandler D, Miller WH. 1999. Semiclassical study of electronically nonadiabatic dynamics in the condensed-phase: spin-boson problem with Debye spectral density. *J. Chem. Phys.* 110(10):4828–40
18. Ananth N, Venkataraman C, Miller WH. 2007. Semiclassical description of electronically nonadiabatic dynamics via the initial value representation. *J. Chem. Phys.* 127(8):084114
19. Miller WH. 2009. Electronically nonadiabatic dynamics via semiclassical initial value methods. *J. Phys. Chem. A* 113(8):1405–15

20. Liu J. 2015. Recent advances in the linearized semiclassical initial value representation/classical Wigner model for the thermal correlation function. *Int. J. Quantum Chem.* 115(11):657–70

21. Church MS, Hele TJH, Ezra GS, Ananth N. 2018. Nonadiabatic semiclassical dynamics in the mixed quantum-classical initial value representation. *J. Chem. Phys.* 148(10):102326

22. Cotton SJ, Miller WH. 2016. The symmetrical quasi-classical model for electronically non-adiabatic processes applied to energy transfer dynamics in site-exciton models of light-harvesting complexes. *J. Chem. Theory Comput.* 12(3):983–91

23. Cotton SJ, Miller WH. 2019. Trajectory-adjusted electronic zero point energy in classical Meyer-Miller vibronic dynamics: symmetrical quasiclassical application to photodissociation. *J. Chem. Phys.* 150(19):194110

24. Cotton SJ, Miller WH. 2019. A symmetrical quasi-classical windowing model for the molecular dynamics treatment of non-adiabatic processes involving many electronic states. *J. Chem. Phys.* 150(10):104101

25. Makri N. 2015. Quantum-classical path integral: a rigorous approach to condensed phase dynamics. *Int. J. Quantum Chem.* 115(18):1209–14

26. Kapral R. 2006. Progress in the theory of mixed quantum-classical dynamics. *Annu. Rev. Phys. Chem.* 57:129–57

27. Huo P, Coker DF. 2012. Semi-classical path integral non-adiabatic dynamics: a partial linearized classical mapping Hamiltonian approach. *Mol. Phys.* 110(9–10):1035–52

28. Agostini F, Abedi A, Suzuki Y, Min SK, Maitra NT, Gross EKU. 2015. The exact forces on classical nuclei in non-adiabatic charge transfer. *J. Chem. Phys.* 142(8):084303

29. Tully JC, Preston RK. 1971. Trajectory surface hopping approach to nonadiabatic molecular collisions: the reaction of H^+ with D_2. *J. Chem. Phys.* 55(2):562–72

30. Tully JC. 1998. Mixed quantum-classical dynamics. *Faraday Discuss.* 110:407–19

31. Wang L, Akimov A, Prezhdo OV. 2016. Recent progress in surface hopping: 2011–2015. *J. Phys. Chem. Lett.* 7(11):2100–12

32. Subotnik JE, Jain A, Landry B, Petit A, Ouyang W, Bellonzi N. 2016. Understanding the surface hopping view of electronic transitions and decoherence. *Annu. Rev. Phys. Chem.* 67:387–417

33. Tully JC. 2012. Perspective: nonadiabatic dynamics theory. *J. Chem. Phys.* 137(22):22A301

34. Hammes-Schiffer S, Tully JC. 1995. Nonadiabatic transition state theory and multiple potential energy surface molecular dynamics of infrequent events. *J. Chem. Phys.* 103(19):8513–27

35. Cao J, Voth GA. 1993. A new perspective on quantum time correlation functions. *J. Chem. Phys.* 99(12):10070–73

36. Cao J, Voth GA. 1994. The formulation of quantum statistical mechanics based on the Feynman path centroid density. II. Dynamical properties. *J. Chem. Phys.* 100(7):5106–17

37. Jang S, Voth GA. 1999. A derivation of centroid molecular dynamics and other approximate time evolution methods for path integral centroid variables. *J. Chem. Phys.* 111(6):2371–84

38. Voth GA. 2007. Path-integral centroid methods in quantum statistical mechanics and dynamics. *Adv. Chem. Phys.* 93:135–218

39. Craig IR, Manolopoulos DE. 2004. Quantum statistics and classical mechanics: real time correlation functions from ring polymer molecular dynamics. *J. Chem. Phys.* 121(8):3368–73

40. Craig IR, Manolopoulos DE. 2005. Chemical reaction rates from ring polymer molecular dynamics. *J. Chem. Phys.* 122(8):084106

41. Habershon S, Manolopoulos DE, Markland TE, Miller TF III. 2013. Ring-polymer molecular dynamics: quantum effects in chemical dynamics from classical trajectories in an extended phase space. *Annu. Rev. Phys. Chem.* 64:387–413

42. Feynman RP, Hibbs AR. 1965. *Quantum Mechanics and Path Integrals*. Mineola, NY: Dover Publ. 1st ed.

43. Chandler D, Wolynes PG. 1981. Exploiting the isomorphism between quantum theory and classical statistical mechanics of polyatomic fluids. *J. Chem. Phys.* 74(7):4078–95

44. Miller TF III. 2008. Isomorphic classical molecular dynamics model for an excess electron in a supercritical fluid. *J. Chem. Phys.* 129(19):194502

45. Menzeleev AR, Miller TF III. 2010. Ring polymer molecular dynamics beyond the linear response regime: excess electron injection and trapping in liquids. *J. Chem. Phys.* 132(3):034106

46. Menzeleev AR, Ananth N, Miller TF III. 2011. Direct simulation of electron transfer using ring polymer molecular dynamics: comparison with semiclassical instanton theory and exact quantum methods. *J. Chem. Phys.* 135(7):074106

47. Boekelheide N, Salomón-Ferrer R, Miller TF III. 2011. Dynamics and dissipation in enzyme catalysis. *PNAS* 108(39):16159–63

48. Kenion RL, Ananth N. 2016. Direct simulation of electron transfer in the cobalt hexammine(II/III) self-exchange reaction. *Phys. Chem. Chem. Phys.* 18(37):26117–24

49. Kretchmer JS, Miller TF III. 2017. Kinetically-constrained ring-polymer molecular dynamics for non-adiabatic chemistries involving solvent and donor–acceptor dynamical effects. *Faraday Discuss.* 195:191–214

50. Ananth N. 2013. Mapping variable ring polymer molecular dynamics: a path-integral based method for nonadiabatic processes. *J. Chem. Phys.* 139(12):124102

51. Duke JR, Ananth N. 2015. Simulating excited state dynamics in systems with multiple avoided crossings using mapping variable ring polymer molecular dynamics. *J. Phys. Chem. Lett.* 6(21):4219–23

52. Pierre S, Duke JR, Hele TJ, Ananth N. 2017. A mapping variable ring polymer molecular dynamics study of condensed phase proton-coupled electron transfer. *J. Chem. Phys.* 147(23):234103

53. Ranya S, Ananth N. 2020. Multistate ring polymer instantons and nonadiabatic reaction rates. *J. Chem. Phys.* 152(11):114112

54. Eklund EC, Ananth N. 2021. Investigating the stability and accuracy of a classical mapping variable Hamiltonian for nonadiabatic quantum dynamics. *Regul. Chaotic Dyn.* 26(2):131–46

55. Richardson JO, Thoss M. 2013. Nonadiabatic ring-polymer molecular dynamics. *J. Chem. Phys.* 139(3):031102

56. Richardson JO, Meyer P, Pleinert MO, Thoss M. 2017. An analysis of nonadiabatic ring-polymer molecular dynamics and its application to vibronic spectra. *Chem. Phys.* 482:124–34

57. Chowdhury SN, Huo P. 2019. State dependent ring polymer molecular dynamics for investigating excited nonadiabatic dynamics. *J. Chem. Phys.* 150(24):244102

58. Chowdhury SN, Huo P. 2021. Non-adiabatic Matsubara dynamics and non-adiabatic ring-polymer molecular dynamics. *J. Chem. Phys.* 154(12):124124

59. Chowdhury SN, Huo P. 2017. Coherent state mapping ring polymer molecular dynamics for non-adiabatic quantum propagations. *J. Chem. Phys.* 147(21):214109

60. Domcke W, Yarkony DR. 2012. Role of conical intersections in molecular spectroscopy and photoinduced chemical dynamics. *Annu. Rev. Phys. Chem.* 63:325–52

61. Liu J. 2016. A unified theoretical framework for mapping models for the multi-state Hamiltonian. *J. Chem. Phys.* 145(20):204105

62. Runeson JE, Richardson JO. 2019. Spin-mapping approach for nonadiabatic molecular dynamics. *J. Chem. Phys.* 151(4):044119

63. Polley K, Loring RF. 2020. Spectroscopic response theory with classical mapping Hamiltonians. *J. Chem. Phys.* 153(20):204103

64. Huo P, Miller TF III, Coker DF. 2013. Predictive partial linearized path integral simulation of condensed phase electron transfer dynamics. *J. Chem. Phys.* 139(15):151103

65. Meyer HD, Miller WH. 1979. Classical models for electronic degrees of freedom: derivation via spin analogy and application to $F^*+H_2 \rightarrow F+H_2$. *J. Chem. Phys.* 71(5):2156–69

66. Nakamura H, Truhlar DG. 2001. The direct calculation of diabatic states based on configurational uniformity. *J. Chem. Phys.* 115(22):10353

67. Baer M. 2002. Introduction to the theory of electronic non-adiabatic coupling terms in molecular systems. *Phys. Rep.* 358(2):75–142

68. Nakamura H, Truhlar DG. 2002. Direct diabatization of electronic states by the fourfold way. II. Dynamical correlation and rearrangement processes. *J. Chem. Phys.* 117(12):5576–93

69. Wu Q, Van Voorhis T. 2006. Constrained density functional theory and its application in long-range electron transfer. *J. Chem. Theory Comput.* 2(3):765–74

70. Sirjoosingh A, Hammes-Schiffer S. 2011. Diabatization schemes for generating charge-localized electron-proton vibronic states in proton-coupled electron transfer systems. *J. Chem. Theory Comput.* 7(9):2831–41

71. Subotnik JE, Alguire EC, Ou Q, Landry BR, Fatehi S. 2015. The requisite electronic structure theory to describe photoexcited nonadiabatic dynamics: nonadiabatic derivative couplings and diabatic electronic couplings. *Acc. Chem. Res.* 48(5):1340–50

72. Yarkony DR, Xie C, Zhu X, Wang Y, Malbon CL, Guo H. 2019. Diabatic and adiabatic representations: electronic structure caveats. *Comput. Theor. Chem.* 1152:41–52

73. Mao Y, Montoya-Castillo A, Markland TE. 2020. Excited state diabatization on the cheap using DFT: photoinduced electron and hole transfer. *J. Chem. Phys.* 153(24):244111

74. Richings GW, Habershon S. 2020. A new diabatization scheme for direct quantum dynamics: Procrustes diabatization. *J. Chem. Phys.* 152(15):154108

75. Trotter HF. 1959. On the product of semi-groups of operators. *Proc. Am. Math. Soc.* 10(4):545–51

76. Suzuki M. 1976. Generalized Trotter's formula and systematic approximants of exponential operators and inner derivations with applications to many-body problems. *Commun. Math. Phys.* 51(2):183–90

77. Chandler D. 1978. Statistical mechanics of isomerization dynamics in liquids and the transition state approximation. *J. Chem. Phys.* 68(6):2959–70

78. Parrinello M, Rahman A. 1984. Study of an F center in molten KCl. *J. Chem. Phys.* 80(2):860

79. Ananth N, Miller TF III. 2010. Exact quantum statistics for electronically nonadiabatic systems using continuous path variables. *J. Chem. Phys.* 133(23):234103

80. Chandler D. 1987. *Introduction to Modern Statistical Mechanics*. Oxford, UK: Oxford Univ. Press

81. Ceperley DM, Jacucci G. 1987. Calculation of exchange frequencies in bcc ^{3}He with the path-integral Monte Carlo method. *Phys. Rev. Lett.* 58(16):1648–51

82. Kubo R. 1957. Statistical mechanical theory of irreversible processes. I. General theory and simple applications to magnetic and conduction problems. *J. Phys. Soc. Jpn.* 12(6):570–86

83. Zwanzig R. 1965. Time-correlation functions and transport coefficients in statistical mechanics. *Annu. Rev. Phys. Chem.* 16:67–102

84. Müller U, Stock G. Flow of zero-point energy and exploration of phase space in classical simulations of quantum relaxation dynamics. II. Application to nonadiabatic processes. *J. Chem. Phys.* 111:77

85. Golosov AA, Reichman DR. 2001. Classical mapping approaches for nonadiabatic dynamics: short time analysis. *J. Chem. Phys.* 114(3):1065–74

86. Habershon S, Manolopoulos DE. 2009. Zero point energy leakage in condensed phase dynamics: an assessment of quantum simulation methods for liquid water. *J. Chem. Phys.* 131(24):244518

87. Hele TJ, Althorpe SC. 2013. Derivation of a true ($t \to 0_+$) quantum transition-state theory. I. Uniqueness and equivalence to ring-polymer molecular dynamics transition-state-theory. *J. Chem. Phys.* 138(8):084108

88. Hele TJ, Althorpe SC. 2013. Derivation of a true ($t \to 0_+$) quantum transition-state theory. II. Recovery of the exact quantum rate in the absence of recrossing. *J. Chem. Phys.* 139(8):084115

89. Althorpe SC. 2021. Path-integral approximations to quantum dynamics. *Eur. Phys. J. B* 94:155

90. Hele TJ. 2013. An electronically non-adiabatic generalization of ring polymer molecular dynamics. arXiv:1308.3950 [physics.chem-ph]

91. Hele TJ, Willatt MJ, Muolo A, Althorpe SC. 2015. Relation of centroid molecular dynamics and ring-polymer molecular dynamics to exact quantum dynamics. *J. Chem. Phys.* 142(19):191101

92. Hele TJ, Ananth N. 2016. Deriving the exact nonadiabatic quantum propagator in the mapping variable representation. *Faraday Discuss.* 195:269–89

93. Hele TJ, Willatt MJ, Muolo A, Althorpe SC. 2015. Boltzmann-conserving classical dynamics in quantum time-correlation functions: "Matsubara dynamics." *J. Chem. Phys.* 142(13):134103

94. Welsch R, Song K, Shi Q, Althorpe SC, Miller TF III. 2016. Non-equilibrium dynamics from RPMD and CMD. *J. Chem. Phys.* 145(20):204118

95. Bonella S, Coker DF. 2003. Semiclassical implementation of the mapping Hamiltonian approach for nonadiabatic dynamics using focused initial distribution sampling. *J. Chem. Phys.* 118(10):4370–85

96. Colbert DT, Miller WH. 1998. A novel discrete variable representation for quantum mechanical reactive scattering via the *S*-matrix Kohn method. *J. Chem. Phys.* 96(3):1982–91

97. Steele RP, Zwickl J, Shushkov P, Tully JC. 2011. Mixed time slicing in path integral simulations. *J. Chem. Phys.* 134(7):074112

98. Coronado EA, Xing J, Miller WH. 2001. Ultrafast non-adiabatic dynamics of systems with multiple surface crossings: a test of the Meyer–Miller Hamiltonian with semiclassical initial value representation methods. *Chem. Phys. Lett.* 349(5–6):521–29

99. Tao X, Shushkov P, Miller TF III. 2019. Simple flux-side formulation of state-resolved thermal reaction rates for ring-polymer surface hopping. *J. Phys. Chem. A* 123(13):3013–20

100. Menzeleev AR, Bell F, Miller TF III. 2014. Kinetically constrained ring-polymer molecular dynamics for non-adiabatic chemical reactions. *J. Chem. Phys.* 140(6):064103

101. Kretchmer JS, Miller TF III. 2016. Tipping the balance between concerted versus sequential proton-coupled electron transfer. *Inorg. Chem.* 55(3):1022–31

102. Duke JR, Ananth N. 2016. Mean field ring polymer molecular dynamics for electronically nonadiabatic reaction rates. *Faraday Discuss.* 195:253–68

103. Mandal A, Yamijala SS, Huo P. 2018. Quasi-diabatic representation for nonadiabatic dynamics propagation. *J. Chem. Theory Comput.* 14(4):1828–40

104. Zhou W, Mandal A, Huo P. 2019. Quasi-diabatic scheme for nonadiabatic on-the-fly simulations. *J. Phys. Chem. Lett.* 10(22):7062–70

105. Habershon S, Fanourgakis GS, Manolopoulos DE. 2008. Comparison of path integral molecular dynamics methods for the infrared absorption spectrum of liquid water. *J. Chem. Phys.* 129(7):074501

106. Horikoshi A, Kinugawa K. 2005. Effective potential analytic continuation approach for real time quantum correlation functions involving nonlinear operators. *J. Chem. Phys.* 122(17):174104

107. Eklund EC, Ananth N. 2020. MAVARIC: a C++ program used to compute Mapping Variable Ring Polymer Molecular Dynamics correlation functions. *MAVARIC*, Version 1.0.0. **https://doi.org/10.5281/zenodo.3900570**